Photometric stellar variation due to extra-solar comets

A. Lecavelier des Etangs, A. Vidal-Madjar, and R. Ferlet

Institut d'Astrophysique de Paris, CNRS, 98bis Boulevard Arago, F-75014 Paris, France

Abstract. We performed numerical simulations of stellar occultations by extra-solar cometary tails. We find that extra-solar comets can be detected by the apparent photometric variations of the central stars. In most cases, the light curve shows a very peculiar "rounded triangular" shape. However, in some other cases, the curve can mimic a planetary occultation. Photometric variations due to comet occultations are mainly achromatic. Nevertheless, if comets with small periastrons have smaller particles, these occultations could be chromatic with a larger extinction in the blue by few percents.

We also estimate the number of detections expected in a large photometric survey at high accuracy. By the observation of several tens of thousand of stars, it should be possible to detect several hundreds of occultation per year. We thus conclude that a spatial photometric survey would detect a large number of extra-solar comets. This would allow to explore the time evolution of cometary activity, and consequently would probe structure and evolution of extra-solar planetary systems.

Key words: occultations – comets: general – stars: planetary systems

1. Introduction

The search for extra-solar planets through photometric variation is a well-known problem analyzed in many aspects for several years (Schneider et al. 1990; Schneider 1996). However, planets are not the only objects detectable by their effect on stars' brightness, comets can also induce photometric variations. In our study of β Pictoris photometric variations (Lecavelier des Etangs et al. 1995), we concluded that the variations observed on November 1981 could be due to the passage in front of the star of either a planet or a dusty cloud (Lecavelier des Etangs et al. 1997, Lamers et al. 1997). If the latter is the correct explanation, this cloud of dust must be a cometary tail for two reasons. First, because the lifetime of the dust in such a system is very short and one must find a way to produce the dust continuously. Second, because the cloud shape is constrained by the observed light curve; the cloud cannot be spherical, it should have a sharp edge in the part pointing toward the star and a huge cloud of dust

---

in the opposite direction: exactly like a cometary tail (Lecavelier des Etangs, 1996).

In the case of the solar system, the observations of stellar occultation by comets have been discussed by Combes et al. (1983). Observations of extinction and polarization of star light by dust of cometary tails in the solar system have been published (Dossin 1962, Ninkov 1994, Rosenbush et al. 1994).

But the solar system is only one particular planetary system at a given age. It is known that cometary activity was formerly much more important, and the well-known case of β Pictoris shows that during the first 10^8 years, a planetary system is expected to show large cometary activity (Ferlet & Vidal-Madjar 1995, Vidal-Madjar et al. 1998). Moreover, presence of comets around stars can be considered as an indirect signature for the presence of gravitational perturbations, and possibly caused by planets.

In this paper, we deal with the important possibility of detecting cometary activity from a photometric survey. We take the COROT space mission as an example of what will be achievable in the very near future (Baglin et al. 1997). COROT, which primary aim is stellar seismology, will be launched in early 2002. It will allow a survey of about 30 000 stars with a photometric accuracy of few 10^{-4} during several months. Here, we predict the probabilities of detecting comets using such a photometric survey.

In Sect 2, we describe the model of the cometary occultation, and then give the expected light curve in Sect. 3. Estimates of the number of comets which could be detected are given in Sect. 4. The conclusion is in Sect. 5.

2. A model of cometary occultation

As pointed out by Lamers et al.(1997), a geometric distribution of the dust must be assumed in order to evaluate the photometric stellar variation due to extra-solar comets. Then, by taking into account the optical properties of the cometary grains, the photometric variation can be estimated.

2.1. Distribution of dust in a cometary tail

The evaluation of the distribution of the dust in a cometary tail can be made through particle simulation. The input parameters are the comet orbit, the dust production rate, the ejection velocity

and the size distribution. We assume a size distribution $dn(s)$ of the form

$$dn(s) = \frac{(1 - s_0/s)^m}{s^n} \tag{1}$$

as observed in the solar system, where s is the dust size. We take $s_0 = 0.1\mu m$, $n = 4.2$, $m = n(s_p - s_0)/s_0$, and $s_p = 0.5\,\mu m$ (Hanner 1983, Newburn & Spinrad 1985). This distribution starts at $s_0 = 0.1\,\mu m$ with $dn(s_0) = 0$, peaks at $s_p = 0.5\,\mu m$, and has a tail similar to a s^{-n} distribution for large sizes.

Dust sensitivity to radiation pressure is given by the β ratio of the radiation force to the gravitational force. We take

$$\beta = 0.2 \left(\frac{L_*/M_*}{L_\odot/M_\odot} \right) \left(\frac{s}{1\,\mu m} \right)^{-1} \tag{2}$$

where L_*/M_* is the luminosity-mass ratio of the star. So the orbits of the small grains are more affected by radiation pressure than those of large grains. This is a very good approximation for particles larger than $0.1\,\mu m$ of any realistic composition and for the solar spectrum (Burns et al. 1979).

The dust production rate P is assumed to vary with r, the distance to the star, and is taken to be

$$P = P_0 \left(\frac{r}{r_0} \right)^{-2} \tag{3}$$

(see, for example, A'Hearn et al., 1995; Weaver et al., 1997, Schleicher et al., 1998). The dust production is taken to be zero beyond 3 AU for a solar luminosity.

As soon as a grain is produced from a comet nucleus, we assume that it is ejected from the parent body with a velocity v_{eject} in an arbitrary direction. The grain then follows a trajectory defined by gravitation and radiation forces. The ejection velocity depends upon the particle size. We take $v_{eject} = \sqrt{\beta}/(A + B\sqrt{\beta})$ (Sekanina & Larson 1984), which approximates the results of Probstein's (1969) two-phase dusty-gas dynamics for the acceleration by the expanding gas within tens of kilometers from the nucleus. The coefficient A and B depend upon many parameters such as the thermal velocity of the expanding gas. We used $A = B = 1\,s\,km^{-1}$ which is a good approximation of different values measured for the comets of the solar system (Sekanina & Larson 1984; Sekanina 1998). This gives an ejection velocity of $\approx 585\,km\,s^{-1}$ for $s = 0.1\,\mu m$. The ejection velocity is smaller for larger grains which have smaller cross section area to mass ratio ($v_{eject}(10\,\mu m) \approx 124\,km\,s^{-1}$). We checked that any other realistic values for A and B give similar light curves within few percents.

2.2. Stellar parameter

The simulations have been performed with the mass, luminosity and radius of the central star set to solar values (M_*, L_* and R_*). Simulation with other parameters could be possible. A larger mass for the central star would induce a shorter time scale; a larger luminosity would increase the effect of the radiation pressure on grains; a larger radius would decrease the relative extinction (Eq. 6). However, the conclusions do not strongly depend on these stellar properties. For instance, adopting the properties of an A5V star does not change the shape of the light curves. By scaling the production rate to the star luminosity, we found a quantitative change by less than a factor of two.

2.3. Grain properties

2.3.1. Extinction

The extinction cross-section of a dust grain is $Q_{ext}(s, \lambda)\pi s^2$, where the extinction efficiency, Q_{ext} is slightly dependent on the particle size (s) and radiation wavelength (λ). If Q_{sca} is the scattering efficiency (see Sect. 2.3.2) and Q_{abs} is absorption efficiency, $Q_{ext}(s, \lambda) = Q_{sca} + Q_{abs}$. We take $Q_{abs} = 1$ if $s \geq \lambda$, and $Q_{abs} = s/\lambda$ if $s < \lambda$, which is a good approximation for optical wavelengths and grains larger than $0.1\,\mu m$ (Draine & Lee 1984).

The total extinction is hence calculated by adding the extinction due to all particles in the line of sight to the star. The optical depth τ due to the dust is

$$\tau = \frac{\sum_{part.} N_{grain/part.} Q_{ext}(s, \lambda)\pi s^2}{S} \tag{4}$$

where S is the projected area of the line of sight. In the simulation, one particle represents an optically thin cloud of several dust grains. The number of physical grains per particle in the simulation, $N_{grain/part.}$, is

$$N_{grain/part.} = \frac{3M_{dust}}{4\pi\rho N_{part.}} \frac{\int dn(s)}{\int s^3 dn(s)} \tag{5}$$

where M_{dust} is the total dust mass, ρ is the dust density, and $N_{part.}$ is the number of particles in the simulation. $N_{part.}$ is set to a few 10^4 in order to keep reasonable computing time.

Because the cometary cloud is optically thick but its size is smaller than the size of the star, we mapped the stellar surface through a set of cells in polar coordinates. For each cell i, we calculate the optical depth τ_i due to the particles within this cell of area S_i ($\sum_i S_i = \pi R_*^2$). The ratio of the flux observed through the cloud (F_{ext}) to the initial stellar flux (F_*) is

$$\frac{F_{ext}}{F_*} = \sum_i \frac{S_i e^{-(\tau_i)}}{\pi R_*^2} \tag{6}$$

The number of cells is the best compromise between the spatial resolution and the number of particles in the simulation. We take into account that the maximum contribution to τ_i by each particle must be $< 10^{-1}$ in order to achieve an accurate result in spite of the quantization of the extinction. S_i and N_{part} are thus constrained by

$$\frac{S_i N_{part}}{10} \geq \frac{3M_{dust} Q_{ext}}{4\rho} \frac{\int s^2 dn(s)}{\int s^3 dn(s)} \tag{7}$$

The limb darkening is not taken into account in this work, because its effect is negligible.

2.3.2. Scattering

As already pointed out by Lamers et al. (1997), the main part of an occulting dust cloud is seen through a very small scattering angle. Thus, the total star light forward-scattered to the observer can be large because the phase function is strongly peaked to small angles for which the diffraction has the dominant contribution. The phase function for the diffraction is[1]

$$P(\theta, \tilde{x}) = \frac{\tilde{x}^2 \left(1 + \cos^2 \theta\right)}{4\pi} \left(\frac{J_1(\tilde{x}\sin\theta)}{\tilde{x}\sin\theta}\right)^2 \tag{8}$$

where $\tilde{x} = 2\pi s/\lambda$. The phase function has been normalized by $\int P(\theta)d\Omega = 1$ and depends upon the wavelength λ. Examples of such phase functions are shown in Lamers et al. (1997).

The scattered light (F_{sca}) is evaluated by adding the contribution of each particle in the simulation.

$$\frac{F_{scat}}{F_*} = N_{\text{grain/part.}} \sum_{\text{part.}} \frac{Q_{sca}\pi s^2 P(\theta)}{r^2} e^{-(\tau_{in}+\tau_{out})}. \tag{9}$$

τ_{in} is the total extinction along the path from the star to the scattering grain and τ_{out} is from the grain to the observer. The grain is at distance r from the star. For $s \geq \lambda$, the scattering efficiency Q_{sca} is assumed to be the diffraction efficiency for large grains: $Q_{sca} = Q_D = 1$ (Pollack & Cuzzi, 1980). For small particles ($s < \lambda$), we used the basic approximation $Q_{sca} = (s/\lambda)^4$ (van de Hulst, 1957). The result is very insensitive to this last assumption because forward scattering at small angle is largely dominated by diffraction on particles larger than the wavelength. Because each cloud represented by a particle is very thin, and the total extinction is small (τ_{in}, $\tau_{out} < 10^{-1}$), we assumed single scattering (no source function).

In fact, for very peaked forward-scattering function on very small scattering angle, the finite size of the star must be taken into account (especially when the dust cloud is seen superimposed on the star surface). Hence, we mapped the stellar surface by small arcs centered on the dust particle. We then calculate the total scattering by adding the contribution of each arc.

3. Light curves

The light observed at a given time is the sum of two opposite effects: the increase of the brightness through the scattering by particles at small angle from the line of sight and the decrease of the brightness through the extinction (including absorption) by particles on the line of sight.

3.1. First order estimations

3.1.1. Extinction

From Eqs. 4 and 5, in the case $s \gtrsim \lambda$ ($Q_{ext} = 2$), and neglecting the inner extinction, we find an upper limit for the extinction:

$$\left(\frac{F_{ext}}{F_*}\right)_{\text{max}} = \exp\left(-\frac{6M_{dust} \int s^2 dn(s)}{4\pi\rho R_*^2 \int s^3 dn(s)}\right) \tag{10}$$

---

[1] The Eq. 12 in Lamers et al. (1997) has a typo-mistake: $\tilde{x}$ in the first fraction must be $\tilde{x}^2$.

For the particle size distribution given by Eq. 1 (Sect. 2.1), we have $(\int s^2 dn(s))/(\int s^3 dn(s)) = 0.15\,\mu^{-1}$. Adopting a dust production of 10^6 kg s^{-1} during 100 days, we find $M_{dust} \approx 10^{13}$ kg. Hence $(\Delta F/F_*)_{\text{max}} \approx 10^{-3}$. This order of magnitude is close to the result of more elaborated calculations (Sect. 3.2). We can already conclude that this variation could be detected by a space photometric survey.

We note that the photometric variations of β Pic in 1981 was $\sim 5\cdot10^{-2}$. The above calculation gives an estimate of the lower limit of the needed production rate: $P \gtrsim 5\cdot10^7$ kg s^{-1}. This is consistent with $P \gtrsim 10^8$ kg s^{-1} obtained from the estimation of Lamers et al. (1997): $P/\Delta v > 10^8$kg km^{-1} and with an assumed relative velocity between the dust and the nucleus of the comet $\Delta v \lesssim 1$ km s^{-1}.

3.1.2. Scattering

If we take a comet at $r = 1$ AU from the star and an impact parameter on the line of sight of one half the stellar radius, then $\theta \approx 7'$. For the particle size distribution given by Eq. 1, the phase function is $\tilde{P}(\theta \approx 7') \approx 700$. Therefore,

$$\frac{F_{scat}}{F_*} \approx \frac{3M_{dust}\tilde{P}(\theta)}{4\rho r^2} \frac{\int s^2 dn(s)}{\int s^3 dn(s)} \approx 4\cdot10^{-5} \tag{11}$$

As a first conclusion, it is clear that both extinction and scattered light can be detected by very precise photometric survey, although scattering gives photometric variations an order of magnitude smaller than extinction. Extinction appears to be the major process observed when the comet is passing in front of the star. This event can thus be called an occultation.

3.2. Light curves

Taking into account the dust spatial distribution and the extinction within the tail, we calculated the light curves of a set of cometary occultations. From a given comet orbit, and dust production rate, we compute the full motion of each dust particle; the result is the variation of the star light as a function of time.

Two typical light curves resulting from the simulation are shown in Fig. 1 and 2. The majority of cometary occultations gives light curves with a very particular "rounded triangular" shape (Fig. 1). This occurs when the dense cometary head first occults the star and gives a very fast and sharp brightness decrease. It is then followed by the tail which gives an additional slow decrease. Similarly, the subsequent brightness increase is also sharp when the cometary head is going out of the occulting part. Then the increase slows down and the brightness returns to the normal level when the cometary tail is less and less dense in front of the star.

However, in some configurations, the tail can be aligned with the line of sight. In these cases the light curves are more symmetric (Fig. 2). They can mimic planetary occultations (Fig. 3). Because of the noise, it will be difficult from such observations to differentiate between a comet and a planet.
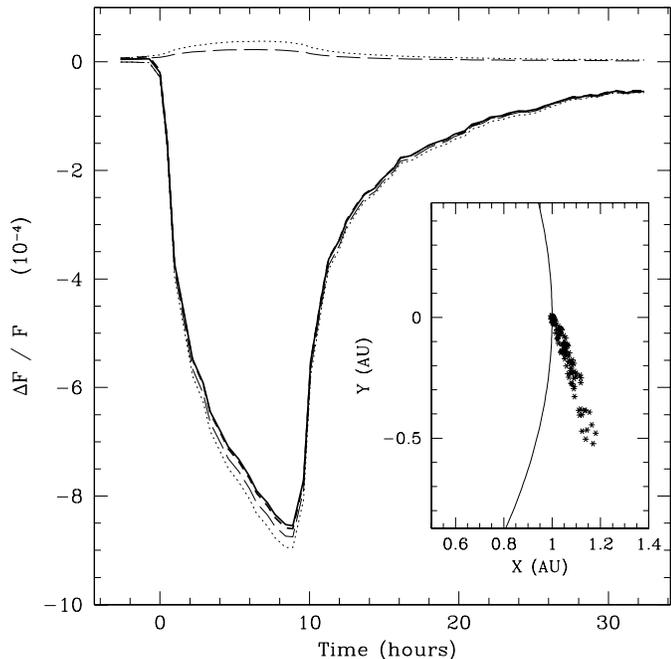
Fig. 1. Plot of the photometric variations during a cometary occultation in red ($\lambda \sim 8000$ Å, thick solid line) and in blue ($\lambda \sim 4000$ Å, thick short-dashed line). The insert is a view from the top when the comet is crossing the line of sight ($Y = 0$) at the periastron. The production rate is $2 \cdot 10^6$ kg s^{-1} at 1 AU. The scattered light is given by the top thin lines, the extinction by the bottom thin lines (long-dashed line for $\lambda \sim 8000$ Å; dotted line for $\lambda \sim 4000$ Å). The total variation is plotted with the thick lines. This light curve presents the very specific "rounded triangular" shape observed in the majority of simulations of cometary occultations. The difference between the variation in the blue and in the red is negligible and less than 1%.

Fig. 2. Same as Fig. 1. Here all the parameters are the same except that the longitude of the periastron is at $90°$ from the line of sight. This gives a production rate of $5 \cdot 10^5$ kg s^{-1} at 2 AU. The cometary tail is aligned with the line of sight; consequently the light curve presents a more symmetrical shape resembling a planetary occultation. The net color effect is hardly detectable and of the order of 1.5%.

3.3. Color signatures

As seen in Sect. 2.3, the light variations show some color signature due to the optical properties of the grains. Particles with a size smaller than the wavelength are less efficient for extinction. Thus, extinction is smaller at larger wavelengths. The forward scattering is more peaked to the small angles at shorter wavelengths (Lamers et al. 1997). The scattering is thus larger at smaller wavelengths when the cometary cloud is occulting the star (*a contrario*, the scattering is larger at larger wavelength when the comet cloud is seen far from the star; but then the scattered light becomes negligible). As a result, there is a balance between the additional scattered light and the extinction; both are larger at smaller wavelengths. It is difficult to predict what will be the color effect on cometary occultation light curves.

In addition, most of the extinction and scattering due to the cometary dust is concentrated in the inner coma, where the number of large particles is larger because smaller particles are more efficiently ejected by radiation pressure (Sect. 2.1). As a consequence, in the optical, and with the size distribution assumed in Sect. 2.1, the light curves are barely dependent on the wavelength (or color band). The difference between variations in blue and in red is smaller than few percents. This color signature
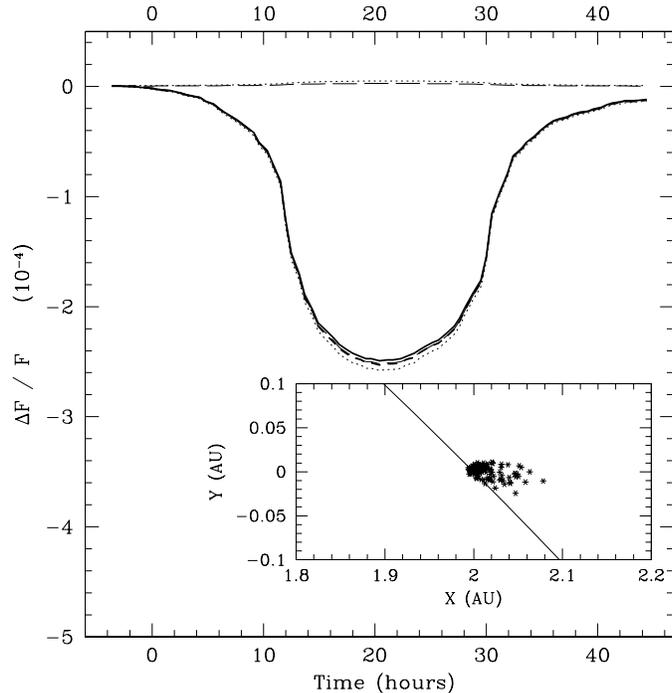
would be very difficult to observe. This is beyond the today technical feasibility.

However, for comets at small distances from the Sun ($\lesssim$ 0.5 AU), its appears that the dust size distribution is peaked at smaller sizes (Newburn & Spinrad 1985). This decrease of a_p with the heliocentric distance could be due to particle fragmentation. Although it is difficult to guess the size distribution for extra-solar comets, it is easy to understand that if small particles are more numerous (with $s < 0.5\,\mu$m), the occultation will show a larger color signature. We checked that a comet with a periastron at 0.3 AU and $s_p = 0.25\,\mu$m (Newburn & Spinrad 1985) gives larger extinction by about 15% in the blue than in the red (Fig. 4).

3.4. Conclusion

Photometric variations due to the stars' occultation by extra-solar comets could be detectable by photometric measurements with an accuracy of $\sim 10^{-3} - 10^{-4}$. In most cases, the particular "rounded triangular" shape of the light curve can be an easy diagnostic for the presence of a comet. However, in some cases, the light curves can mimic an occultation by a more compact object like a classical extra-solar planet (Lecavelier des Etangs et al. 1997). The color signatures of cometary occultations can be too small to avoid the confusion. The detection of periodicity appears to be critical in the diagnostic of a planetary occultation.
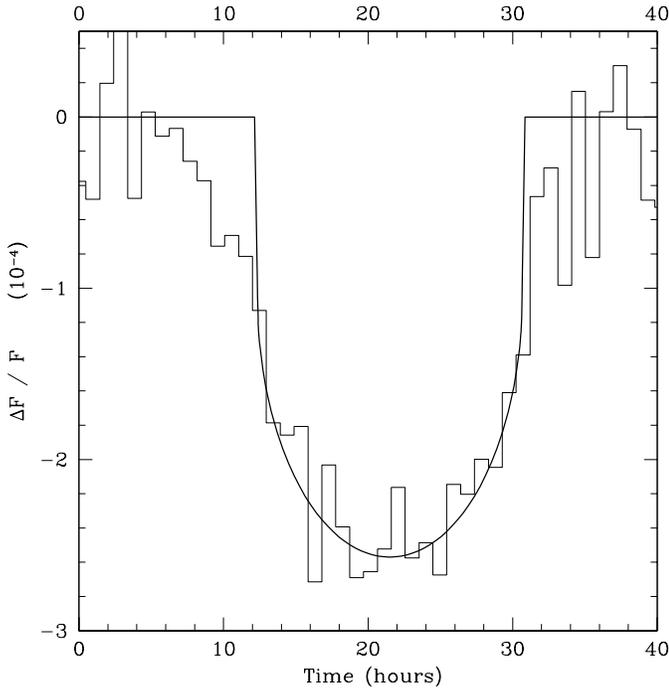
Fig. 3. Plot of the photometric variations due to a comet similar to the comet of the Fig. 2 (histogram). Here the result is given as a noisy observation with a photometric measurement every hour and an accuracy of $3\sigma = 10^{-4}$. For comparison, an occultation by a planet with a radius of 9 000 km and orbiting at 2 AU is plotted with limb darkening effect taken into account (thick line). The detected variation is very similar to a planetary occultation, the main difference being extended wings in the cometary case.

Alternatively, the polarization is another way to discriminate the two *phenomena*, because the light is scattered by the cometary dust roughly gathered in the same plane. But, with a level of at most few percents in polarization of solely the scattered light, this gives $< 0.01\%$ polarization in total and would also be difficult to detect. In cases of planetary and cometary occultations, spectroscopic follow-up observations should be planned to allow a better analysis of a suspected on-going detection.

4. Probability of detection

From the above modeling, we can evaluate the probability to detect a photometric stellar variation due to an extra-solar comet. We assume a survey of a given number of stars at a given accuracy. We carried out a large number of simulations of cometary occultations in all directions.

4.1. Orbital parameters

The characteristics of the comets are given by their distribution in the parameter space. Concerning the orbital parameters, the periastron density distribution is chosen to be the same as the one observed in the solar system: $dn(q) \propto q^{0.3}dq$ with $q \in [0.1\,\mathrm{AU}, 2\,\mathrm{AU}]$ (A'Hearn et al., 1995). Many sun-grazing comets have been discovered by SOHO with perihelion $q < 0.1$ AU
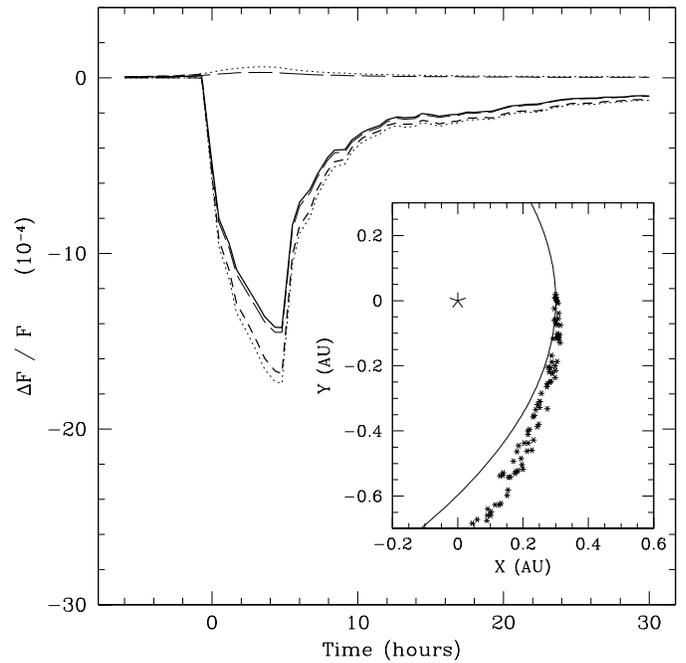

Fig. 4. Same as Fig. 1. Here all the parameters are the same except that the periastron is at 0.3 AU and the particle size distribution is taken with $a_p = 0.25\,\mu$m. The production rate corresponds to $2 \cdot 10^7$ kg s^{-1} at 0.3 AU. Because there are more particles smaller than the wavelength, we see a dipper occultation in the blue by about 15%.

(Kohl et al. 1997; see also the numerous IAU Circulars). But it is still difficult to infer the distribution for these small periastrons. The above distribution is thus likely biased by an underestimate of the number of comets with small periastron, because such comets are difficult to observe. These star-grazing comets give a larger photometric variation. Therefore, we possibly slightly underestimate the probabilities of detection.

We fixed all the apoastrons at 20 AU, the longitudes of periastron, the ascending nodes and the inclinations are chosen randomly.

4.2. Dust production rate

One of the most important parameter is the dust production rate. Because, it dictates the mass of dust in the tail, and constrains the detectability of the comet. The amplitude of the photometric variation is roughly proportional to that parameter.

We consider that the dust production rate (P) is proportional to the area of the comet's nucleus, and that the distribution of the comets' radii (R_c) is similar to the distribution observed for the comets, asteroids, and Kuiper belt objects of the solar system. We assume that the number density of objects with radius in the range R_c to $R_c + dR_c$ is $dn(R_c) \propto R_c^{-\gamma}dR_c$. γ is a positive number, typically in the range 3 to 4 (Luu 1995). It is constrained to be ~ 3–3.5 for the comets' nuclei observed with $R \in [0.1\,\mathrm{km}, 100\,\mathrm{km}]$ (Fernández 1982, Hughes & Daniels 1982, Brandt et al. 1997) The same distribution is consistent with the observation of the Kuiper belt objects: $\gamma \sim 3$ with
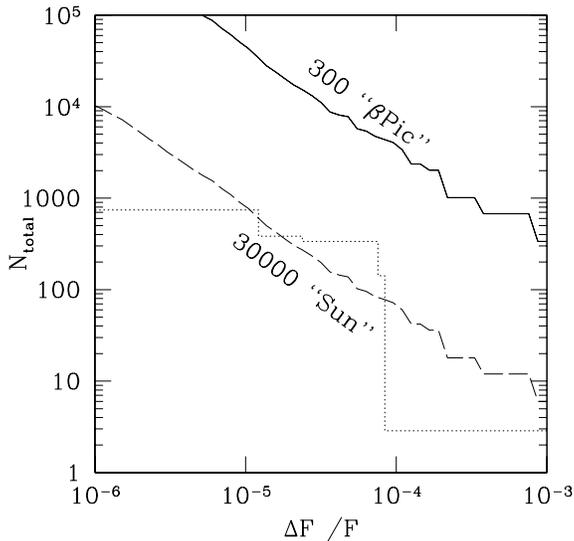
Fig. 5. Plot of the number of detections of cometary occultations as a function of the photometric accuracy. Two cases are considered: the "pessimistic case" which is a survey of $n_{star} = 30000$ sun-like stars, during $T_{obs} = 1$ year ($n_{comet} = 100$, $P_0 = 10^3$ kg s^{-1}), and the "optimistic case" where among the 30000 stars, 1% ($n_{star} = 300$) have a β Pictoris-like activity ($n_{comet} = 100$, $P_0 = 10^6$ kg s^{-1}). With an accuracy of 10^{-4}, about 10 to 10^3 detections can be expected. The large difference between the two cases shows that this kind of survey will also give information on the planetary evolution. For comparison, the dotted histogram gives the number of detection of planets assuming that each star has a planetary system like the solar system. With an accuracy larger than 10^{-4}, this gives the number of detection of giant planets, and mainly Jupiter-like planets. With an accuracy better than 10^{-4}, Earth-like planets will be detected. Each step in the histogram represents the possibility to detect successively the Earth ($8 \cdot 10^{-5}$), Venus ($7 \cdot 10^{-5}$), Mars ($2 \cdot 10^{-5}$) and Mercury (10^{-5}). We see that accurate photometric survey should detect more comets than planets.

$R \in [100 \text{ km}, 400 \text{ km}]$ (Jewitt 1996), or with theoretical models for the formation of these objects: $\gamma \sim 4$ for $R \lesssim 200$ km (Kenyon & Luu, 1998). With the assumption that $P \propto R_c^2$, the number of comets with a production rate between P and $P+dP$ is $dn(P) \propto P^{-(\gamma+1)/2}dP$. We adopt $\gamma = 3.5$. Changing γ to 3 or 4 would change the probability of detection by less than a factor of two.

Finally, this distribution is normalized by n_{comet}, the number of comets per unit of time passing through the periastron with a production rate larger than P_0. Hence, we have $n_{comet} \propto \int_{P_0}^{\infty} dn(P)$. Thus,

$$n_{comet} \propto P_0^{(1-\gamma)/2}. \tag{12}$$

4.3. Results

Using a large number of various comets, we calculate the probability of detection at a given photometric accuracy. Then, the number of possible detections is simply this probability multiplied by n_{comet}, the duration of the observation T_{obs} and the number of stars surveyed n_{star}.

We suppose that the time scale between each measurement is small enough ($\lesssim 1$ hour) that each variation above the detection limit will effectively be detected. As an example, we take $T_{obs} = 1$ year and $n_{star} = 30\,000$, which is the order of magnitude for the future space mission COROT.

The expected number of detections is plotted in Fig. 5. We considered two types of planetary systems. The first one is similar to the solar system with $n_{comet} = 100$ comets per year with $P \geq P_0 = 10^3$ kg s^{-1} at $r_0 = 1$ AU. We see that few dozens of comets could be detected at an accuracy of 10^{-4}. We consider it as the pessimistic case.

The second type of planetary system is supposed to be a young planetary system with a large cometary activity as during the youth of the solar system. The typical example is the well-known star β Pictoris where comets' infalls are commonly observed through UV and optical spectroscopy (see e.g., Ferlet et al. 1987, Lagrange et al. 1988, Beust et al. 1990, Vidal-Madjar et al. 1994, 1998). For such a planetary system, $n_{comet} = 100$ comets per year with $P \geq P_0 = 10^6$ kg s^{-1} at $r_0 = 1$ AU (Beust 1995, Beust et al. 1996). Note that β Pictoris is young but on the main sequence (Crifo et al. 1997), its age is few percents of the age of the solar system. Therefore, in a set of 30 000 stars there should be about $n_{star} \approx 300$ stars with about the same activity as β Pictoris. Thus, few thousands comets could be expected with a survey at 10^{-4} accuracy. We consider it as the optimistic case.

The solar system is likely not exceptional. The bottom-line in Fig. 5 is a good estimate of the lower limit of the expected number of detections. Younger stars may have a higher level of activity, with a larger number of comets; but, although infrared excess have been observed around many main sequence stars, β Pictoris is certainly a very peculiar case (Vidal-Madjar et al. 1998). Thus, the top-line in Fig. 5 gives a good estimate of the upper limit of the expected number of detections.

Note that the major assumption that the dust production rates in the solar system can be extrapolated to large values is realistic. A large rate has effectively been observed in the recent comet Hale-Bopp where it reached of few times 10^5 kg s^{-1} at about 1 AU (Rauer H. et al., 1997, Schleicher et al., 1997, Senay et al. 1997, Weaver et al., 1997).

It is very likely that in the near future a large number of extra-solar comets will be detected through occultations.

For comparison, we also evaluate the probability to detect planets assuming that each star has a planetary system like the solar system. With an accuracy better than 10^{-2}, Jupiter can be detected. Below 10^{-3}, other giant planets are also detectable. But because of their large orbital periods, their contribution to the number of detections is smaller than the one from Jupiter. With a total probability of $\sim 10^{-4}$ to detect a giant planet in one year, the survey of 30000 stars will give ~ 3 planets. With an accuracy better than 10^{-4}, Earth-like planets start to be detectable. Because of their smaller distance to the star, they have larger contribution to the probability of planet detection. The Earth and Venus can be detected with a probability of $\sim 10^{-2}$ in one year. Mars and Mercury, which are detectable with an accuracy of $\sim 10^{-5}$, give a total probability of $\sim 3 \cdot 10^{-2}$. The

comparison with the number of detection of comets shows that accurate photometric surveys should detect more comets than planets.

5. Conclusion

We performed detailed numerical simulations of stars' occultations by extra-solar comets. We extracted the apparent photometric variations of the central stars due to these putative comets. We have shown that:

1) Extra-solar comets can be detected through photometric variations due to occultation by dusty tails. In many cases, the light curve shows a very particular "rounded triangular" shape. However, in some remaining cases, the curve can mimic a planetary occultation.

2) The photometric variations due to cometary occultations are mainly achromatic. This property will allow to discriminate the occultations by comets from intrinsic stellar variations. However, the confusion with planetary occultations cannot be efficiently removed by color measurements in the optical.

3) The number of detections which can be expected from a large photometric survey of several tens of thousand of stars at high accuracy (10^{-4}) is of the order of several hundreds of occultations per year.

These detections will allow to explore the evolution of the cometary activity through the correlation with the stellar age. Indeed, we know from the solar system exploration that the cometary activity significantly changed with time. Moreover, comets are believed to be the primitive bricks of the planetary formation, and planets perturbation are needed to push them toward the central star. It is thus clear that the detection and analysis of the cometary activity around nearby stars will give important information on the structure and evolution of the planetary systems.

References

A'Hearn M.F., Millis R.L., Schleicher D.G., Osip D.J., Birch R.V., 1995, Icarus 118, 223

Baglin A., Auvergne M., Bare P., et al., 1997, In: Schull M. (ed.) NASA Origins Conference

Beust H., 1995, In: Ferlet R., Vidal-Madjar A. (eds.) Circumstellar Dust Disk and Planet Formation. Editions Frontières, p. 35

Beust H., Lagrange-Henri A.M., Vidal-Madjar A., Ferlet R., 1990, A&A 236, 202

Beust H., Lagrange A.M., Plazy F., Mouillet D., 1996, A&A 310, 181

Brandt J., Randall C., Stewart I., et al., 1997, BAAS 191, 3303

Burns J., Lamy P., Soter S., 1979, Icarus 40, 1

Combes M., Lecacheux J., Encrenaz T., et al., 1983, Icarus 56, 229

Crifo F., Vidal-Madjar A., Lallement R., Ferlet R., Gerbaldi M., 1997, A&A 320, L29

Dossin F., 1962, Annales de l'Observatoire de Haute-Provence 45, 30

Draine B.T., Lee H.M., 1984, ApJ 285, 89

Ferlet R., Hobbs L.M., Vidal-Madjar A., 1987, A&A 185, 267

Ferlet R., Vidal-Madjar A., 1995, Circumstellar Dust Disk and Planet Formation. Editions Frontières

Fernández J.A., 1982, AJ 87, 1318

Hanner M.S., 1983, In: Gombosi T.I. (ed.) Cometary exploration II. CRIP Budapest, p. 1

Hughes D.W., Daniels P.A., 1982, MNRAS 198, 573

Jewitt D., 1996, AJ 112, 1225

Kenyon S.J., Luu J.X., 1998, AJ, in press

Kohl J.L., Noci G., Cranmer S.R., 1997, BAAS 191, 7309

Lagrange A.M, Vidal-Madjar A., Ferlet R., 1988, A&A 190, 275

Lamers H.J.G.L.M., Lecavelier des Etangs A., Vidal-Madjar A., 1997, A&A 328, 321

Lecavelier des Etangs A., 1996, Thèse de l'Université Paris VII

Lecavelier des Etangs A., Deleuil M., Vidal-Madjar A., et al., 1995, A&A 299, 557

Lecavelier des Etangs, A., Vidal-Madjar A., Burki G., et al., 1997, A&A 328, 311

Luu J., 1995, In: Ferlet R., Vidal-Madjar A. (eds.) Circumstellar Dust Disk and Planet Formation. Editions Frontières, p. 195

Newburn R.L., Spinrad H., 1985, AJ 90, 2591

Ninkov Z., 1994, AJ 107, 1182

Pollack J.B., Cuzzi J.N., 1980, Journ. Atmos. Sc. 37, 868

Probstein R.F., 1969, In: Bisshopp F., et al. (eds.) Problems of Hydrodynamics and Continuum Mechanics. Society of Industrial and Applied Mathematics, p. 568

Rauer H., Arpigny C., Boehnhardt H., et al., 1997, Sci 275, 1909

Rosenbush V.K., Rosenbush A.E., Dement'ev M.S., 1994, Icarus 108, 81

Schleicher D.G., Lederer S.M., Millis R.L., Farnham T.L., 1997, Sci 275, 1913

Schleicher D.G., Millis R.L., Birch P.V., 1998, Icarus 132, 397

Schneider J., 1996, Ap&SS 241, 35

Schneider J., Chevreton M., Martin E.L., 1990, In: Formation of Stars and Planets, and the Evolution of the Solar System. p. 67

Sekanina Z., 1998, ApJ 494, L121

Sekanina Z., Larson S.M., 1984, AJ 89, 1408

Senay M., Rownd B., Lovell A., et al., 1997, BAAS, DPS meeting 29, 32.06

van de Hulst H.C., 1957, Light Scattering by Small Particles. Wiley

Vidal-Madjar A., Lagrange-Henri A.M., Feldman P.D., et al., 1994, A&A 290, 245

Vidal-Madjar A., Lecavelier des Etangs A., Ferlet R., 1998, Planet. Space Sci. 46, 629

Weaver H.A., Feldman P.D., A'Hearn M.F., et al., 1997, Sci 275, 1900